

From spirals to dwarf irregulars: a new tight scaling relation linking the gas and stellar content of galaxies to disc gravitational instability

Alessandro B. Romeo^{1*}

¹*Department of Space, Earth and Environment, Chalmers University of Technology, SE-41296 Gothenburg, Sweden*

Accepted Received; in original form

ABSTRACT

We present a new galaxy scaling relation that predicts the mass fractions of atomic gas, molecular gas and stars as a function of fundamental physical properties such as mass and specific angular momentum. Our scaling relation stretches across two orders of magnitude in mass fraction, and applies to galaxies of any morphological type from Sa to dIrr, thus spanning five orders of magnitude in stellar mass. It has a 1σ scatter of 0.2 dex, a correlation coefficient of 0.8 and a significance level close to 0, which means that the correlation between measured and predicted mass fractions is tight, strong and significant. The new scaling relation is not a best-fitting relation and has no free parameters, but originates from the low galaxy-to-galaxy variance of $\langle Q \rangle$, the mass-weighted average of Toomre’s Q stability parameter. This is in contrast to the variance/variation of Q within a galaxy, which is particularly large for atomic gas.

Key words: instabilities – stars: kinematics and dynamics – ISM: kinematics and dynamics – galaxies: ISM – galaxies: kinematics and dynamics – galaxies: star formation.

1 INTRODUCTION

Statistical correlations between physical properties of galaxies are indispensable tools for unravelling the fundamental laws that govern galaxy formation and evolution across the observed variety of scales. Such ‘scaling relations’ are therefore constantly used for testing simulation and semi-analytic models of galaxy evolution, and for constraining their predictions (e.g., Dutton et al. 2011; Lagos et al. 2016; Agertz et al. 2019). Recent examples of galaxy scaling relations that have attracted special interest are those linking the mass fractions of atomic and molecular gas to stellar mass, or to related properties like stellar mass surface density, specific star formation rate and colour (e.g., Saintonge et al. 2011; Huang et al. 2012; Boselli et al. 2014; Catinella et al. 2018).

Recent investigations focusing on spiral galaxies suggest that the observed scaling relation between the mass fraction of atomic gas and stellar mass could be driven by disc gravitational instability. Obreschkow et al. (2016) proposed a hybrid stability model that predicts the mass fraction of atomic (hydrogen+helium) gas as a function of mass and specific angular momentum of the whole (gas+stars) disc, assuming a constant HI velocity dispersion: $f_{\text{HI}} = \min\{1, 2.5 q^{1.12}\}$, where $q = j_{\text{disc}} \sigma_{\text{HI}} / GM_{\text{disc}}$ and $\sigma_{\text{HI}} = 10 \text{ km s}^{-1}$. Such a

stability model has been tested in a variety of applications (e.g., Lagos et al. 2017; Lutz et al. 2017, 2018; Stevens et al. 2018; Wang et al. 2018; Džudžar et al. 2019; Murugesan et al. 2019; Stevens et al. 2019). Another important contribution is the one by Zasov & Zaitseva (2017), who showed that the relation between atomic gas mass and disc specific angular momentum is equally well described by a simpler stability model controlled by Q_{gas} , the gas Toomre parameter, assuming that Q_{gas} is approximately constant within a galaxy (like σ_{gas}). This stability model was tested and further constrained by Kurapati et al. (2018).

Romeo & Mogotsi (2018) pointed out that q and Q_{gas} are not fully reliable stability diagnostics because stars, and not atomic or molecular gas, are the primary driver of disc instabilities in spiral galaxies (Romeo & Mogotsi 2017), which is true even for a powerful starburst+Seyfert galaxy like NGC 1068 (Romeo & Fathi 2016). A more reliable diagnostic is $\langle Q_{\star} \rangle$, the mass-weighted average of the stellar Toomre parameter, which allowed us to tightly constrain the relation between stellar mass, stellar specific angular momentum and disc stability level (Romeo & Mogotsi 2018).

This Letter goes deeper and wider. It shows *the* route that connects Toomre’s Q stability parameter to the mass fraction of *each* baryonic component in the disc, and presents a new scaling relation that illustrates such a link for disc-dominated galaxies of *all* morphological types.

* E-mail: romeo@chalmers.se

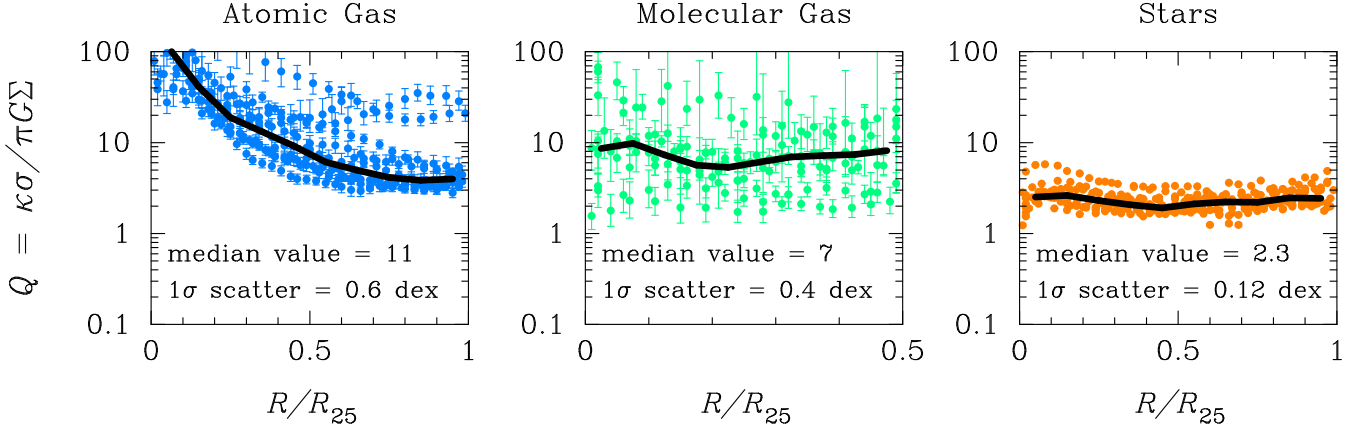


Figure 1. Radial profiles of the Toomre parameter for L08’s sample of spirals, with the galactocentric distance measured in units of the optical radius (B-band isophotal radius at 25 mag arcsec⁻²). Also shown is the local median of Q . In the case of molecular gas, the radial range is limited by the sparsity of sensitive CO measurements beyond half the optical radius.

2 THE BIG PICTURE

2.1 From Q to f_{pred} , the predicted mass fractions

To explore the link between disc gravitational instability and the gas and stellar content of galaxies, we start from the simplest stability diagnostic: the Toomre (1964) parameter, $Q = \kappa\sigma/\pi G\Sigma$. It is commonly assumed that $Q \approx 1$, consistent with a process of self-regulation that keeps galaxy discs close to marginal stability (see sect. 1 of Krumholz et al. 2018 for an overview). How realistic is that assumption? To answer this question, we analyse a sample of 12 nearby star-forming spirals, originally selected and analysed by Leroy et al. (2008), hereafter L08: NGC 628, 2841, 3184, 3198, 3351, 3521, 3627, 4736, 5055, 5194, 6946 and 7331. These are galaxies with sensitive and spatially resolved measurements across the entire optical disc, including reliable radial profiles of the H I and CO velocity dispersions (Romeo & Mogotsi 2017).

Fig. 1 illustrates that atomic gas (H I), molecular gas (H₂) and stars (★) have distinct radial distributions of Q , which differ both in median trend and in variance. While Q_{\star} is quite close to unity, Q_{H_2} is three times more offset and scattered, whereas $Q_{\text{H I}}$ exhibits a two-orders-of-magnitude decline within the optical radius and an even larger median offset from unity than Q_{H_2} . Such a diversity results from the complex interplay between the heating and cooling processes that regulate the value of Q in galaxy discs (Krumholz & Burkert 2010; Forbes et al. 2012, 2014, 2018), and from the fact that $Q_{\text{H I}}$, Q_{H_2} and Q_{\star} do not really measure the stability levels of atomic gas, molecular gas and stars. $Q_{\text{H I}}$, Q_{H_2} and Q_{\star} are instead the building blocks of a more realistic, multi-component Q stability parameter (Romeo & Falstad 2013). Such a parameter is dominated by Q_{\star} because stars, and not molecular or atomic gas, are the primary driver of disc instabilities in spiral galaxies (Romeo & Fathi 2016; Romeo & Mogotsi 2017; Marchuk 2018; Marchuk & Sotnikova 2018). This is the reason why Q_{\star} is much closer to the critical stability level ($Q_{\text{crit}} \approx 2\text{--}3$) than Q_{H_2} or $Q_{\text{H I}}$. Note that Q_{crit} is higher than unity, but its precise value is still questioned (Romeo & Fathi 2015). In fact, Q_{crit} is influenced by complex phenomena such as non-axisymmetric

perturbations (e.g., Griv & Gedalin 2012) and gas dissipation (Elmegreen 2011), whose effects are difficult to evaluate.

Now that we have clarified how self-regulated galaxy discs are, let us analyse how the Toomre parameter of component i , $Q_i = \kappa\sigma_i/\pi G\Sigma_i$, varies from galaxy to galaxy. To suppress the variation of Q_i within a galaxy, we take the mass-weighted average of $Q_i(R)$:

$$\langle Q_i \rangle = \frac{1}{M_i(R_{\text{av}})} \int_0^{R_{\text{av}}} Q_i(R) \Sigma_i(R) 2\pi R dR. \quad (1)$$

This type of average is especially useful because it relates $\langle Q_i \rangle$ to fundamental galaxy properties such as mass, M_i , and specific angular momentum, $j_i = J_i/M_i$, via a simple and accurate approximation (Romeo & Mogotsi 2018). The resulting relation is $\langle Q_i \rangle \propto \mathcal{A}_i$, where

$$\mathcal{A}_i = \frac{j_i \bar{\sigma}_i}{GM_i}, \quad (2)$$

$$j_i = \frac{1}{M_i} \int_0^{\infty} R v_c(R) \Sigma_i(R) 2\pi R dR, \quad (3)$$

$$\bar{\sigma}_i = \frac{1}{R_{\text{av}}} \int_0^{R_{\text{av}}} \sigma_i(R) dR. \quad (4)$$

Note two points concerning Eqs (1)–(4):

- M_i and j_i are the total mass and the total specific angular momentum of atomic hydrogen+helium gas ($i = \text{H I}$), molecular hydrogen+helium gas ($i = \text{H}_2$) or stars ($i = \star$);
- while $\langle Q_i \rangle$ is the mass-weighted average of $Q_i(R)$, $\bar{\sigma}_i$ is the radial average of $\sigma_i(R)$, where σ denotes the radial velocity dispersion.

Note also that the coefficient of proportionality between $\langle Q_i \rangle$ and \mathcal{A}_i is not well defined for a component whose mass distribution is far from exponential, like atomic gas (e.g., Bigiel & Blitz 2012). In view of that, we opt for a unified approach and use \mathcal{A}_i as a proxy for $\langle Q_i \rangle$: it is well defined for all the components, and it is simpler than $\langle Q_i \rangle$. In addition, the offset of \mathcal{A}_i from $\langle Q_i \rangle$ is not an issue, since $Q_i = 1$ no longer means marginal stability when the disc has multiple, gravitationally coupled components (Romeo & Falstad 2013; see also Fig. 1 and its discussion).

To compute the \mathcal{A}_i stability parameter for L08’s sample

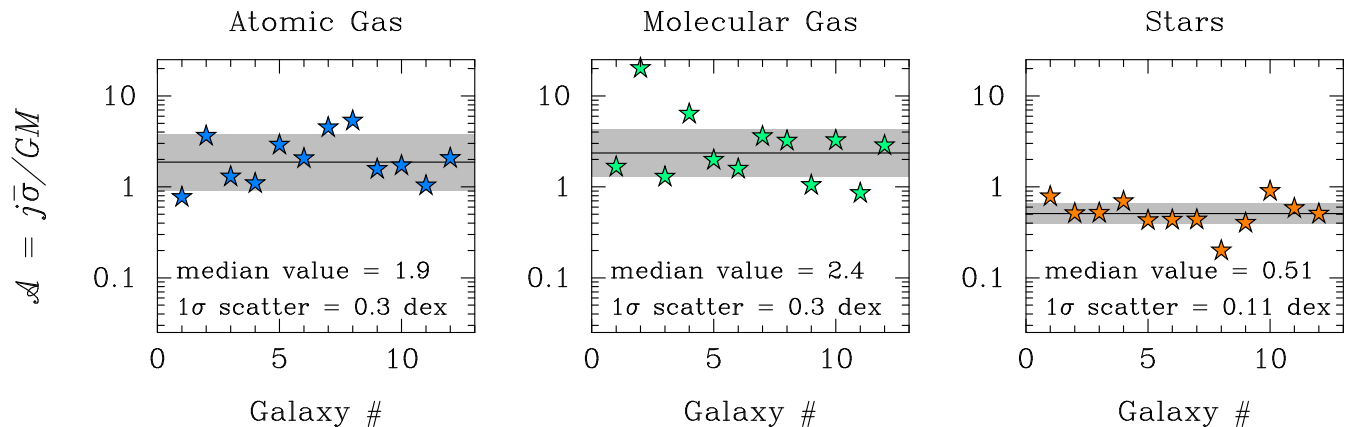


Figure 2. Galaxy-to-galaxy variation of the \mathcal{A} stability parameter for L08’s sample of spirals (the galaxy list is given in the first paragraph of Sect. 2.1). Also shown are the median value and 1σ scatter of \mathcal{A} .

of spirals, we use the values of M_i and j_i tabulated by L08 and Obreschkow & Glazebrook (2014), respectively. We also need to evaluate $\bar{\sigma}_i$, hence to choose the averaging radius R_{av} . Although one can do that arbitrarily, we prefer to make use of all the information provided by the σ_i measurements. Therefore we choose $R_{av} = R_{25}$ for atomic gas, $R_{av} = \frac{1}{2}R_{25}$ for molecular gas and $R_{av} = R_{25}$ for stars, where R_{25} is the optical radius (B-band isophotal radius at 25 mag arcsec $^{-2}$). In the case of molecular gas, the radial range is limited by the sparsity of sensitive CO measurements beyond half the optical radius (see fig. 1 of Romeo & Mogotsi 2017 and its discussion).

Fig. 2 shows that the 1σ scatter of \mathcal{A}_i ranges from 0.1 dex, the small value measured for stars, to 0.3 dex, the value measured for molecular and atomic gas.¹ This means that the median of \mathcal{A}_i over the galaxy sample provides a reliable estimate of the value of \mathcal{A}_i in each galaxy: $\mathcal{A}_i \approx \mathcal{A}_{med\ i}$. This relation, which is accurate to within 30% (0.1 dex) for the stellar component and a factor of 2 (0.3 dex) for the gas components, is more far-reaching than it looks. Consider $\mathcal{A}_{med\ i}$ as known, replace \mathcal{A}_i with the right-hand side of Eq. (2), and multiply by $f_i = M_i/M_{disc}$, the mass fraction of component i ($M_{disc} = M_\star + M_{HI} + M_{H2}$). The resulting relation is $f_i \approx f_{pred\ i}$, where

$$f_{pred\ i} = \frac{j_i \hat{\sigma}_i}{GM_{disc}} \quad (5)$$

and $\hat{\sigma}_i \equiv \bar{\sigma}_i/\mathcal{A}_{med\ i}$. This result speaks clearly: if we know $C_i = 1/\mathcal{A}_{med\ i}$, then we can accurately predict the gas and stellar content of spiral galaxies as a function of disc gravitational instability. In our case $C_{HI} = 0.5$, $C_{H2} = 0.4$ and $C_\star = 2.0$ (see Fig. 2). But suppose that one chooses other values of R_{av} , for instance because reliable σ_i measurements are available only within the inner optical disc. In this case look at Table 1, where C_i is calibrated for various choices of R_{av} using L08’s sample of spirals, and compute $\hat{\sigma}_i$ as

¹ This is the scatter from galaxy to galaxy, σ_{gg} , which can be combined with the total scatter given in Fig. 1, σ_{tot} , to estimate the rms scatter of Q_i within a galaxy: $\sigma_g = \sqrt{\sigma_{tot}^2 - \sigma_{gg}^2}$. Specifically, $\sigma_g = 0.5, 0.2$ and 0.05 dex for atomic gas, molecular gas and stars, respectively. In the text, we focus on a more important meaning of σ_{gg} .

Table 1. The atomic-gas (H1), molecular-gas (H2) and stellar (\star) C -factors appearing in Eq. (6) for various choices of the averaging radius (R_{av}), measured in units of either the stellar half-mass/light radius (R_{50}) or the B-band isophotal radius at 25 mag arcsec $^{-2}$ (R_{25}). In the case of molecular gas, the radial range is limited by the sparsity of sensitive CO measurements beyond half the optical radius. These C -factors are used in Sect. 2.2 for populating the f - f_{pred} plot (Fig. 3).

R_{av}	C_{HI}	C_{H2}	C_\star
1.0 R_{50}	0.4	0.4	1.2
1.5 R_{50}	0.4	0.4	1.4
2.0 R_{50}	0.5	—	1.7
2.5 R_{50}	0.5	—	1.9
3.0 R_{50}	0.6	—	2.2
0.5 R_{25}	0.4	0.4	1.4
1.0 R_{25}	0.5	—	2.0

$$\hat{\sigma}_i = C_i \bar{\sigma}_i, \quad (6)$$

where $\bar{\sigma}_i$ is given by Eq. (4). The expected accuracy of our prediction is instead independent of R_{av} .

What if there are no σ_i measurements available at all? We can predict f_i even in such a case, although with lower accuracy. In fact, Eq. (5) is still valid provided that $\hat{\sigma}_i$ is redefined as $\hat{\sigma}_i \equiv (\bar{\sigma}/\mathcal{A})_{med\ i}$, the median of $\bar{\sigma}_i/\mathcal{A}_i$ over the galaxy sample. Once again, we calibrate this quantity using L08’s sample of spirals:

$$\hat{\sigma}_i = \begin{cases} 11 \text{ km s}^{-1} & \text{if } i = \text{H1}, \\ 8 \text{ km s}^{-1} & \text{if } i = \text{H2}, \\ 130 \text{ km s}^{-1} \times (M_\star/10^{10.6} M_\odot)^{0.5} & \text{if } i = \star. \end{cases} \quad (7)$$

In $\hat{\sigma}_\star$ we have incorporated the approximate scaling $\bar{\sigma}_\star \propto M_\star^{0.5}$ (Romeo & Mogotsi 2018; Gilhuly et al. 2019), which is measured across spiral galaxies of any given type (Sa–Sd) and stellar mass ($M_\star = 10^{9.5}–10^{11.5} M_\odot$).

2.2 The new scaling relation

To test the accuracy of our prediction and illustrate the new scaling relation, $f_i = j_i \hat{\sigma}_i / GM_{disc}$, we analyse 101 galaxies, from spirals to dwarf irregulars, spanning five orders of magnitude in M_\star , three and a half orders of magnitude in M_{HI} ,

and three orders of magnitude in $M_{\text{H}2}$. Such galaxies belong to five distinct samples, which we name and describe below.

(i) ‘Sp (L08+)’ is the sample analysed in Sect. 2.1. It contains 12 spirals of type Sab–Sc from the THINGS, HERACLES and SINGS surveys. For these galaxies there are published measurements of M_{HI} , $M_{\text{H}2}$ and M_{\star} (L08), j_{HI} , $j_{\text{H}2}$ and j_{\star} (Obreschkow & Glazebrook 2014), σ_{HI} and $\sigma_{\text{H}2}$ (Romeo & Mogotsi 2017), and σ_{\star} (L08). Hence we predict f_{HI} , $f_{\text{H}2}$ and f_{\star} using Eqs (5) and (6).

(ii) ‘Sp (RM18+)’ contains 34 spirals of type Sa–Sd from the EDGE-CALIFA survey. For these galaxies there are published measurements of $\langle Q_{\star} \rangle_{50}$, the mass-weighted average of $Q_{\star}(R)$ over the stellar half-light radius (Romeo & Mogotsi 2018), M_{\star} and $M_{\text{H}2}$ (Bolatto et al. 2017). There is also a compilation of H I masses kindly provided by Alberto Bolatto and Tony Wong in advance of publication (the sources for the spectra are: van Driel et al. 2001; Springob et al. 2005; Courtois et al. 2009; Haynes et al. 2011; Masters et al. 2014; Wong et al., in preparation). For consistency with the analysis carried out in Sect. 2.1, we convert stellar masses from the Salpeter initial mass function (IMF) assumed by the CALIFA team (Cid Fernandes et al. 2013; Sánchez et al. 2016) to the Kroupa IMF assumed by L08, i.e. we divide M_{\star} and multiply $\langle Q_{\star} \rangle_{50}$ by 1.6. We then divide $\langle Q_{\star} \rangle_{50}$ by 3.6 to get \mathcal{A}_{\star} , and finally use Eqs (5) and (6) to predict f_{\star} .

(iii) ‘sp (L08+)’ contains 4 small spirals of type Sc–Scd from the THINGS, HERACLES and SINGS surveys. For these galaxies there are published measurements of M_{HI} , $M_{\text{H}2}$ and M_{\star} (L08), j_{HI} , $j_{\text{H}2}$ and j_{\star} (Obreschkow & Glazebrook 2014), and σ_{\star} (L08). Hence we predict f_{HI} and $f_{\text{H}2}$ using Eqs (5) and (7), and f_{\star} using Eqs (5) and (6).

(iv) ‘sp–dw (E17)’ contains 9 small late-type spirals and 28 dwarf irregulars from the WHISP survey. For these galaxies there are published measurements of M_{HI} , M_{\star} , j_{HI} and j_{\star} (Elson 2017). We neglect the contribution of molecular gas to M_{disc} , like Elson (2017), and predict f_{HI} and f_{\star} using Eqs (5) and (7).

(v) ‘dw (B17)’ contains 14 dwarf irregulars from the LITTLE THINGS survey. For these galaxies there are published measurements of M_{HI} , M_{\star} , j_{HI} and j_{\star} (Butler et al. 2017). We neglect the contribution of molecular gas to M_{disc} , like Butler et al. (2017), and predict f_{HI} and f_{\star} using Eqs (5) and (7).

Fig. 3 illustrates that the new scaling relation, $f_i = j_i \hat{\sigma}_i / GM_{\text{disc}}$, stretches across two orders of magnitude in f_i , and applies not only to spirals of type Sa–Sd but also to dwarf irregulars. This is surprising, considering that such a relation has no free parameters and has been predicted analysing a single representative sample of spirals [Sp (L08+)]. To quantify the tightness, strength and significance of the correlation between f_i and $j_i \hat{\sigma}_i / GM_{\text{disc}}$, we present the results of four statistical measures and associated tests. First of all, we measure the dispersion of the data points around the predicted scaling relation using robust statistics: $\text{SD}_{\text{rob}} = 1/0.6745 \text{ MAD}$, where SD_{rob} is the robust counterpart of the standard deviation and MAD is the median absolute deviation (see, e.g., Müller 2000). The resulting 1σ scatter is 0.23 dex, which is precisely the 1σ scatter predicted using a single representative galaxy sample [Sp (L08+)]. This number means a tight correlation. Secondly, we measure Pearson’s r , Spearman’s ρ and Kendall’s

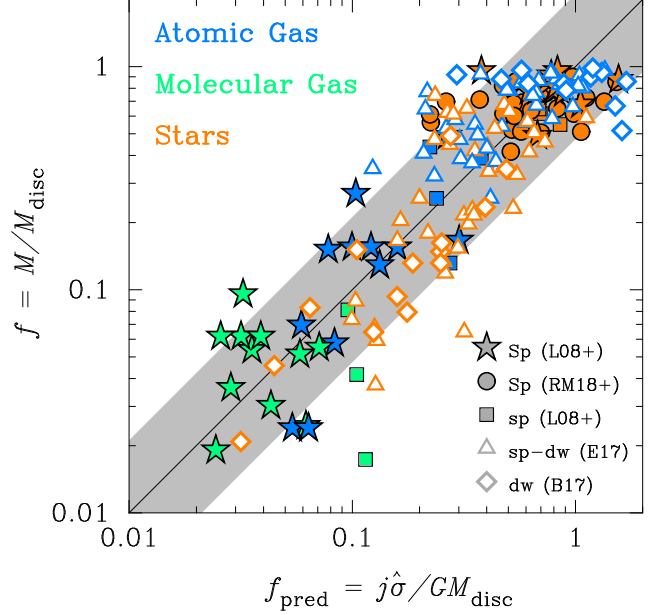


Figure 3. Measured (f) versus predicted (f_{pred}) mass fractions of atomic gas, molecular gas and stars for L08’s sample of spirals (star symbols), and for the other galaxy samples described in Sect. 2.2. Also shown are the predicted scaling relation, $f = j\hat{\sigma}/GM_{\text{disc}}$ (black line), and the predicted 1σ scatter, 0.23 dex (grey area). Note that 82% of the data points fall within the grey area, thus highlighting the accuracy of our prediction.

τ correlation coefficients, together with their significance levels p_r , p_ρ and p_τ (see, e.g., Press et al. 1992). We find that: $r = 0.83$, $\rho = 0.82$, $\tau = 0.62$; $p_r, p_\rho, p_\tau \lesssim 10^{-36}$. These numbers mean a strong and significant correlation.

3 CONCLUSIONS

- This Letter demonstrates that there is a measurable link between the mass fraction of each baryonic component in the disc of a galaxy, f_i , and disc gravitational instability. The key quantity behind such a link is $\langle Q_i \rangle$, the mass-weighted average of Toomre’s Q_i stability parameter. The resulting scaling relation predicts f_i as a function of j_i , the specific angular momentum of that baryonic component, $\hat{\sigma}_i$, a properly redefined velocity dispersion, and M_{disc} , the mass of the disc (see Eq. 5). One can make use of our scaling relation whether there are reliable velocity dispersion measurements (see Eq. 6) or not (see Eq. 7). This Letter also demonstrates the wide range of applicability (Sa–dIrr) and the tightness (0.2 dex) of such a relation.

- The fact that the new scaling relation has a wide range of applicability means, in particular, that it is able to predict f_{HI} and f_{\star} in dwarf irregulars, i.e. down to masses as low as $M_{\text{HI}} \approx 10^7 M_{\odot}$ and $M_{\star} \approx 10^6 M_{\odot}$. Let us illustrate the accuracy of our predictions with an eloquent example: compare the LITTLE THINGS measurements shown in Fig. 3 [dw (B17)] with the corresponding measurements shown in fig. 2 of Obreschkow et al. (2016). In our case 79% of the measurements fall within ± 0.2 dex from the predicted scaling relation, whereas in their case only 29% of the H I measurements do so: the rest of them queue along the $f_{\text{HI}} = 1$

line, where the prediction gives up by imposing an upper limit on f_{HI} (Obreschkow et al. 2016 do not predict f_{\star}). This highlights, once again, the usefulness of our scaling relation.

• Last but not least, the tightness of the new scaling relation originates from the low galaxy-to-galaxy variance of $\langle Q_i \rangle$. This should not be confused with the variance/variation of Q_i within a galaxy, which is another important aspect of the problem. In spiral galaxies, for instance, Q_{HI} exhibits a two-orders-of-magnitude median decline within the optical radius, whereas $\langle Q_{\text{HI}} \rangle$ shows a 1σ scatter of 0.3 dex. At the other extreme we find Q_{\star} , which has a total 1σ scatter of 0.1 dex, i.e. Q_{\star} is approximately constant both within a galaxy and from galaxy to galaxy. These and the other statistical measurements presented in this Letter impose tight constraints on how self-regulated galaxy discs are, and will thus put new-generation models of star formation and/or galaxy evolution to a stringent test.

ACKNOWLEDGEMENTS

We are very grateful to Alberto Bolatto and Tony Wong for providing us with a compilation of HI masses that they made for galaxies from the EDGE-CALIFA survey (see the references listed in item ii of Sect. 2.2), and to Ed Elson for providing us with measurements of mass and specific angular momentum that he made for galaxies from the WHISP survey (Elson 2017). In addition, we are very grateful to Oscar Agertz, Alberto Bolatto, Françoise Combes, John Forbes, Mark Krumholz and Claudia Lagos for useful discussions.

REFERENCES

Agertz O. et al., 2019, preprint (arXiv:1904.02723)
 Bigiel F., Blitz L., 2012, ApJ, 756, 183
 Bolatto A. D. et al., 2017, ApJ, 846, 159
 Boselli A., Cortese L., Boquien M., Boissier S., Catinella B., Lagos C., Saintonge A., 2014, A&A, 564, A66
 Butler K. M., Obreschkow D., Oh S.-H., 2017, ApJ, 834, L4
 Catinella B. et al., 2018, MNRAS, 476, 875
 Cid Fernandes R. et al., 2013, A&A, 557, A86
 Courtois H. M., Tully R. B., Fisher J. R., Bonhomme N., Zavodny M., Barnes A., 2009, AJ, 138, 1938
 Dutton A. A. et al., 2011, MNRAS, 416, 322
 Džudžar R. et al., 2019, MNRAS, 483, 5409
 Elmegreen B. G., 2011, ApJ, 737, 10
 Elson E. C., 2017, MNRAS, 472, 4551
 Forbes J., Krumholz M., Burkert A., 2012, ApJ, 754, 48
 Forbes J. C., Krumholz M. R., Burkert A., Dekel A., 2014, MNRAS, 438, 1552
 Forbes J. C., Krumholz M. R., Speagle J. S., 2018, preprint (arXiv:1810.12919)
 Gilhuly C., Courteau S., Sánchez S. F., 2019, MNRAS, 482, 1427
 Griv E., Gedalin M., 2012, MNRAS, 422, 600
 Haynes M. P. et al., 2011, AJ, 142, 170
 Huang S., Haynes M. P., Giovanelli R., Brinchmann J., 2012, ApJ, 756, 113
 Krumholz M., Burkert A., 2010, ApJ, 724, 895
 Krumholz M. R., Burkert B., Forbes J. C., Crocker R. M., 2018, MNRAS, 477, 2716
 Kurapati S., Chengalur J. N., Pustilnik S., Kamphuis P., 2018, MNRAS, 479, 228
 Lagos C. d. P. et al., 2016, MNRAS, 459, 2632

Lagos C. d. P., Theuns T., Stevens A. R. H., Cortese L., Padilla N. D., Davis T. A., Contreras S., Croton D., 2017, MNRAS, 464, 3850
 Leroy A. K., Walter F., Brinks E., Bigiel F., de Blok W. J. G., Madore B., Thornley M. D., 2008, AJ, 136, 2782 (L08)
 Lutz K. A. et al., 2017, MNRAS, 467, 1083
 Lutz K. A. et al., 2018, MNRAS, 476, 3744
 Marchuk A. A., 2018, MNRAS, 476, 3591
 Marchuk A. A., Sotnikova N. Y., 2018, MNRAS, 475, 4891
 Masters K. L., Crook A., Hong T., Jarrett T. H., Koribalski B. S., Macri L., Springob C. M., Staveley-Smith L., 2014, MNRAS, 443, 1044
 Müller J. W., 2000, J. Res. Natl. Inst. Stand. Technol., 105, 551
 Murugesan C., Kilborn V., Obreschkow D., Glazebrook K., Lutz K., Džudžar R., Dénes H., 2019, MNRAS, 483, 2398
 Obreschkow D., Glazebrook K., 2014, ApJ, 784, 26
 Obreschkow D., Glazebrook K., Kilborn V., Lutz K., 2016, ApJ, 824, L26
 Press W. H., Teukolsky S. A., Vetterling W. T., Flannery B. P., 1992, Numerical Recipes in Fortran: The Art of Scientific Computing. Cambridge University Press, Cambridge
 Romeo A. B., Falstad N., 2013, MNRAS, 433, 1389
 Romeo A. B., Fathi K., 2015, MNRAS, 451, 3107
 Romeo A. B., Fathi K., 2016, MNRAS, 460, 2360
 Romeo A. B., Mogotsi K. M., 2017, MNRAS, 469, 286
 Romeo A. B., Mogotsi K. M., 2018, MNRAS, 480, L23
 Saintonge A. et al., 2011, MNRAS, 415, 32
 Sánchez S. F. et al., 2016, Rev. Mex. Astron. Astrofis., 52, 171
 Springob C. M., Haynes M. P., Giovanelli R., Kent B. R., 2005, ApJS, 160, 149
 Stevens A. R. H., Lagos C. d. P., Obreschkow D., Sinha M., 2018, MNRAS, 481, 5543
 Stevens A. R. H. et al., 2019, MNRAS, 483, 5334
 Toomre A., 1964, ApJ, 139, 1217
 van Driel W., Marcum P., Gallagher III J. S., Wilcots E., Guidoux C., Monnier Ragaïgne D., 2001, A&A, 378, 370
 Wang L. et al., 2018, ApJ, 868, 93
 Wong T. et al., in preparation
 Zasov A. V., Zaitseva N. A., 2017, Astron. Lett., 43, 439

This paper has been typeset from a \LaTeX file prepared by the author.